JOURNAL OF MATERIALS SCIENCE 25 (1990) 3029–3033

Defects restoration during cooling and annealing in PTC type barium titanate ceramics

TSAI-FA LIN, CHEN-TI HU
Department of Materials Science and Engineering, National Tsing Hua University, Hsinchu, Taiwan 30043,

I-NAN LIN
Chun-Shan Institute of Science and Technology, Lungtan, Taiwan,

The PTC-type $BaTiO_3$ ceramics of similar microstructure are obtained by careful control of a sintering scheme. The defect chemistry of them is modified by varying the cooling rate and annealing conditons. In addition to applying Heywang and Jonker models for explaining the resistivity anomaly of these samples, the outward diffusion of oxygen vacancies (V_O), which left excess barium vacancies (V_{Ba}) behind, is proposed to be the formation mechanism of surface states. The formation of defect complex consisting of a $V_O^{\cdot\cdot}$–V_{Ba}'' pair is assumed to be the cause of small diffusivity of V_O in these materials. The phenomena, in which the slower cooling rate raises the resistivity of samples, is ascribed to the higher concentration of excess barium vacancies (V_{Ba}) contained in these samples. However, the maximum potential barrier height (ϕ_{max}) of the samples is the same, irrespective of the amount of surface state concentration (N_s) and is estimated to be $\phi_{max} = 0.66$ eV, from the ln (ρ_{max})–$1/T_{max}$ plot.

1. Introduction

Since the positive temperature coefficient of resistivity (PTCR) characteristics of donor-doped barium titanate ceramics was discovered [1], great efforts have been made to understand the conduction mechanism [2–10], formation mechanism [11–14] and application [15–17] of these materials. Nowadays, ceramics with good PTCR performance have been produced via careful control of processing parameters, and widely applied in many thermoelectric devices. As to the conduction mechanisms, the Heywang and Jonker models [3, 4] are generally accepted to explain the resistivity anomaly. The Heywang [3] model proposed that the potential barrier arising from the electron-trapping effect of the surface states on the grain boundaries results in high resistivity of the specimen at elevated temperature. Jonker [4] modified this model by proposing the compensation of surface states due to spontaneous polarization, which occurs at the ferroelectric state, to account for low resistivity of PTCR ceramics at the temperature below the Curie point (T_c).

While these models satisfactorily explain the temperature dependence of resistivity, the genuine sources of surface state is still not well understood. Daniels *et al.* [8] postulated that the inward diffusion of barium vacancies near the grain boundaries plays the roles of an electron trap; Jonker [4, 18] and Heywang [19] assumed that the adsorption of oxygen atoms and segregation of impurities, respectively, at grain boundaries act as the surface states. Owing to the complexity of the conduction mechanism, the electrical properties of PTC-type $BaTiO_3$ ceramics are very sensitive to both microstructure and defect chemistry of the samples, which, in turn, are significantly affected by the processing parameters such as chemical composition [20–22], sintering condition [23, 24] and heat-treatment [25, 26], etc.

In this study, the sintering scheme is carefully controlled such that the microstructures of the samples are similar to each other. The defect chemistry of the materials is then modified by means of various cooling and annealing processes. The influence of defect chemistry on the PTCR behaviour of $BaTiO_3$ ceramics can thus be identified, and the defect restoration during cooling and annealing will be discussed.

2. Experimental procedures

The PTC materials were prepared by the conventional mixing-oxide procedure. The raw materials $BaCO_3$, TiO_2, Sb_2O_3 and Al_2O_3–SiO_2–TiO_2(AST) in a ratio of 4 : 9 : 3 of reagent grade purity (Riedel-de Haën, West Germany), were weighted according to the formula $BaTi_{1.005}O_{3.01}$ + 0.15% Sb_2O_3 + 5.3% AST. These powders were mixed in an alumina ball mill for 12 h with deionized water, then calcined at 1000° C for 2 h and pulverized for 4 h. The AST is employed to provide a homogeneous and stable microstructure via the mechanism of liquid phase sintering [27].

After granulation by passing through a 60 mesh powder sieve, the powders were pressed into discs (12 mm diameter and 2.2 mm thickness) under a pressure of about 90 MPa. All of the samples were sintered in air at 1350° C for 2 h but with the cooling procedure strictly controlled. The cooling was conducted at 10, 33, 100, 300, 900° C h^{-1}, and quenching, respectively. All the samples were annealed at 600° C for 40 min in

0022–2461/90 $03.00 + .12

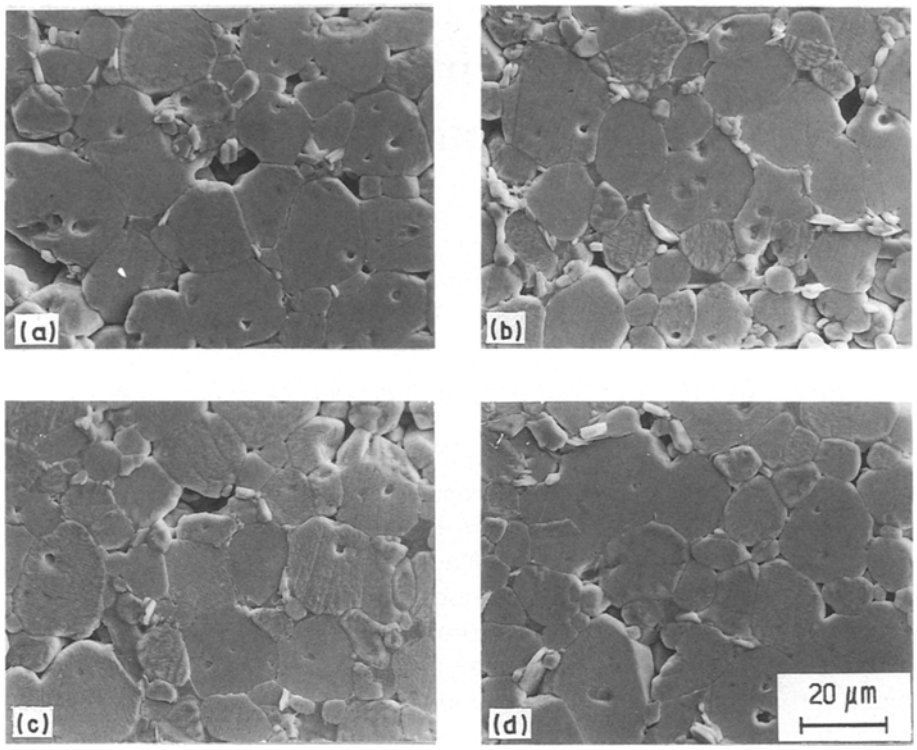

Figure 1 The micrographs of polished and thermally etched surface of the sample sintered at 1350° C for 2 h and cooled at the rate of (a) 10° C h^{-1}, (b) 100° C h^{-1}, (c) 900° C h^{-1} and (d) quenching.

air to study the corresponding effect on the electrical properties. Additional heat treatments, i.e. 1000° C in air for 10 to 250 min, were conducted before the said annealing process (600° C for 40 min) for quenched samples. After plating with electroless-nickel as electrodes, the d.c. resistivity–temperature (ρ–T) characteristics of the samples were measured. The microstructure was observed using a scanning electron microscope (JOEL, JCXA-733). The complex impedance technique was employed to determine the intrinsic resistivity of grains, using an impedance analyser (Hewlett Packard, HP 4192A). The details of the technique have been described elsewhere [28].

3. Results

The microstructure of samples is not significantly influenced by the cooling rate (α_c) in the sintering process and the subsequent annealing procedure. The typical micrographs shown in Fig. 1 illustrate that all the granular structure is similar in density ($\approx 90\%$ of theoretical density), grain size ($\approx 20\,\mu$m) and size distribution, irrespective of the cooling condition. The similarity in microstructure for all samples shows that the modification of electrical properties arises from the effect of defect restoration in the samples.

The effects of cooling rate (α_c) on the ρ–T characteristics of PTC-type $BaTiO_3$ ceramics are demonstrated in Fig. 2. Both the room-temperature and high-temperature resistivities of the samples decrease with the increase of α_c value, when the cooling rate of the specimens is slower than 300° C h^{-1} (full curves). The cooling rate also modifies the shape of the ρ–T curve markedly. The resistivity anomaly rises sharply at T_c and drops rapidly after the maximum for the 10° C h^{-1} cooled sample. Both the resistivity jump at T_c and declination after maximum resistivity (ρ_{max}) occur at a less steep rate as the cooling rate (α_c) increases. Moreover, the temperature corresponding to the maximum resistivity (T_{max}) shifts toward the higher end for samples cooled at a faster rate. Further increase in cooling rate does not significantly modify the ρ–T characteristics, which is shown as a broken curve in Fig. 2 for the 900° C h^{-1} cooled sample. Small value of ρ_{max} accompanied with the poor PTCR behaviour are observed for the quenched samples (chain curve in Fig. 2).

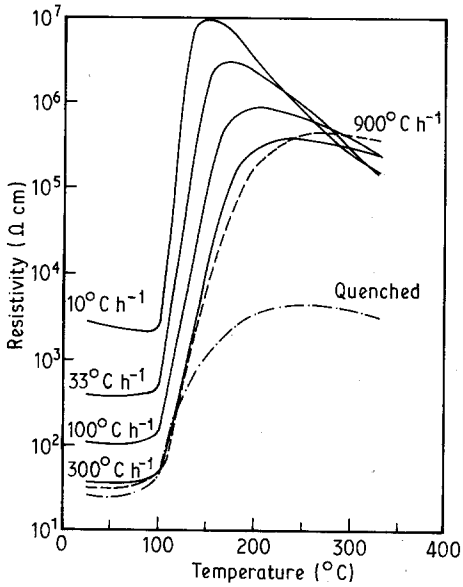

Figure 2 The resistivity–temperature characteristics of the samples sintered at 1350° C for 2 h and cooling at different rates; 10° C h^{-1}, 33° C h^{-1}, 100° C h^{-1} and 300° C h^{-1} (full curves), 900° C h^{-1} (broken curve), and quenched (chain curve).

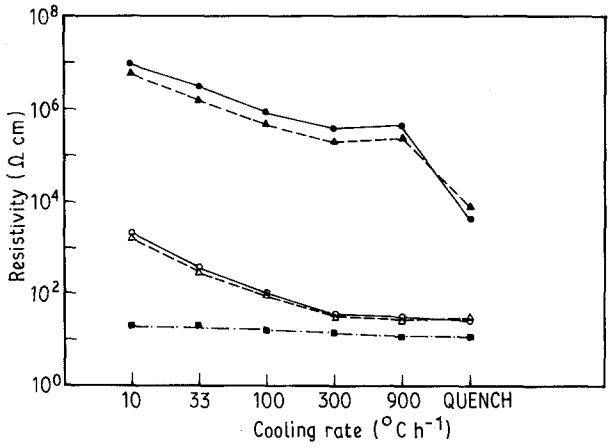

Figure 3 The maximum and minimum resistivities of the samples before (full curves) and after (broken curves) 600° C annealing, and the intrinsic grain resistivities obtained from complex impedance analysis (chain curve). (● ρ_{max}, ▲ ρ_{max} (600° C, 40 min), ○ ρ_{min}, △ ρ_{min} (600° C, 40 min), ■ ρ_0).

The influences of cooling rate on the electrical behaviour are summarized in Fig. 3. Both the minimum and maximum resistivities (ρ_{min} and ρ_{max}) of the samples in Fig. 2 are plotted against the cooling conditions of the samples (full curves). It is interesting to note that the PTCR jump (ρ_{max}/ρ_{min}) is almost unchanged, about four orders of magnitude although ρ_{min} and ρ_{max} decrease simultaneously as the cooling rate increases. Furthermore, ρ_{min} remains at about 30 Ω cm for the samples cooled faster than 300° C h^{-1}. The intrinsic resistivity of the grain interior (ρ_0) of the samples is estimated from the result of the complex impedance measurement and is the value obtained from the extrapolation of the resistance–reactance (R–X) curves toward high frequency end. The ρ_0 value of all the samples is the same ($\approx$ 10 Ω cm), irrespective of their cooling conditions, and is plotted as a chain curve in Fig. 3. This result reveals that the mechanism by which the cooling rate influences the electrical properties (ρ_{max} and ρ_{min}) of these samples is through the modification of defect chemistry in the regions near the grain boundaries rather than via the changes of resistivity in the interior of the grains.

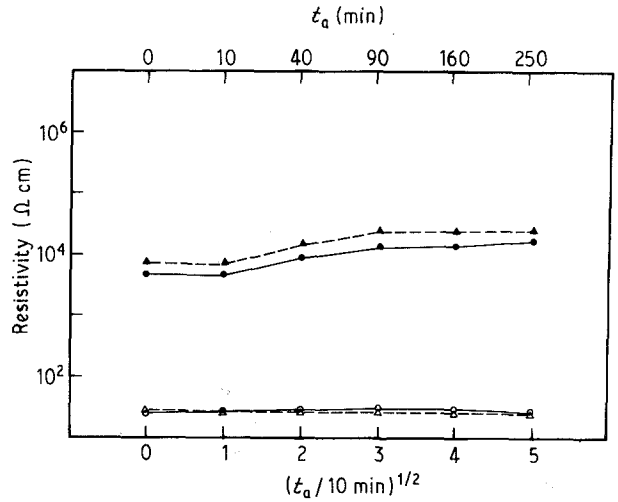

Figure 4 Effect of 1000° C annealing (full curves) and 600° C annealing (broken curves) on the ρ_{max} and ρ_{min} of the quenched samples. (● ρ_{max}, ▲ ρ_{max} (600° C, 40 min) ○ ρ_{min}, △ ρ_{min} (600° C, 40 min)).

Low temperature annealing (600° C for 40 min) decreases the ρ_{min} and ρ_{max} of all samples slightly except for the quenched ones, as indicated by the broken curves in Fig. 3. High temperature annealing (1000° C) on the quenched samples, unexpectedly, only increases the high temperature resistivity moderately. The prolonging of annealing time (t_a) imposes only a minor effect on the improvement of the PTCR behaviour of the samples (full curves in Fig. 4). Re-annealing at low temperature (600° C) after these samples are quenched from 1000° C increases the ρ_{max} further (broken curves in Fig. 4). The ρ_{min}, on the other hand, only changed by a negligible amount for both the annealing processes.

4. Discussion

According to the Heywang's model [3], the apparent resistivity of PTC samples is related to the potential barrier height ϕ existing at grain boundaries by the following equation

$$\rho = \alpha\rho_0 \exp(\phi/kT) \quad (1)$$

where α and ρ_o are the geometrical factor and resistivity of the grains, respectively and k and T are Boltzmann constant and measuring temperature (K), respectively. The potential barrier height ϕ, on the other hand is related to the surface states existing at grain boundaries and the other intrinsic electronic parameters of the grains. The correlation between these parameters can be simplified as

$$\phi = \frac{e^2 N s^2}{2\varepsilon_0 \varepsilon_r N_D} \quad (2)$$

where e is the electronic charge, N_s the concentration of effective surface states, N_D the concentration of ionized donors, ε_0 the permittivity of vacuum, and ε_r the relative permittivity (dielectric constant). The temperature dependence of the dielectric constant above T_c follows the Curie–Weiss law, i.e.

$$\varepsilon_r = \frac{C}{T - T_c}$$

where C is the Curie constant and T_c the Curie point.

When the temperature increases above T_c, the barrier height ϕ will rise rapidly due to the abrupt drop of ε_r. The apparent resistivity, thereafter, increases exponentially with the temperature. As the potential barrier bends upward, the energy level of the surface states (E_s) also increases relative to the Fermi level (E_F), since the energy level of the surface states E_s is fixed relative to the bottom of the conduction band. Re-emission of trapped electrons from the surface states will occur as the E_s is raised over the Fermi level (E_F). The increase in ϕ due to the lowering of ε_r is thus suppressed by the decrease in surface state concentration N_s (cf. Equation 2). The potential barrier, therefore, reaches its maximum value (ϕ_{max}) at the moment that the surface state level E_s touches the Fermi level (E_F) and $\phi_{max} = E_s - E_F$. Whenever the nature of the surface states, or the E_s value, of the samples is the same, the maximum potential barrier height ϕ_{max} of the samples will be the same too, no

matter how high the concentration of surface states N_s is.

A larger surface state concentration (N_s) results in a higher potential barrier, ϕ, according to Equation 2. The surface state level E_s is thus closer to the Fermi level (E_F) and the potential barrier will reach its maximum value more quickly after the temperature passes T_c. On the other hand, lower N_s corresponds to smaller ϕ and E_s is further away from E_F. The potential barrier will approach its maximum at a higher ($T - T_c$) value. This is demonstrated qualitatively in Fig. 2. Recalling that the electric resistivity of PTC samples is related to the potential barrier ϕ through Equation 1, the maximum potential barrier height ϕ_{max} can thus be expressed as

$$\frac{\phi_{max}}{kT_{max}} = \ln\left(\frac{\rho_{max}}{\rho_0}\right) - \ln \alpha \qquad (3)$$

The plot of ln (ρ_{max}/ρ_0) against $1/T_{max}$ as shown in Fig. 5 is observed to fit a straight line surprisingly well for data corresponding to the samples cooled at a rate from 10 to 300° C h^{-1}. This result infers that the ϕ_{max} values of these samples are the same which, in turn, indicates that the potential barrier arises from the surface state of the same nature (i.e. E_s value). Only the concentration of surface states N_s varies with the cooling rate. The faster the cooling rate the lower the N_s will be. The maximum potential barrier height of these samples is estimated to be $\phi_{max} = 0.66$ eV. The fact that the data of 900° C h^{-1} cooled and quenched samples do not fall on the same straight line could be caused by the alteration of the nature of surface state and needs to be investigated further.

As for the mechanism of the formation of surface states, although the inward diffusion of barium vacancies (V_{Ba}) proposed by Daniels [8] explained successfully the formation of carrier depletion layer in the grain boundary region, it can not explain the results of our observation. As shown in Fig. 4, the ρ_{max} of quenched samples increases only moderately when they are annealed at 1000° C for 10 to 250 min (full curve) and increases further by 600° C annealing for 40 min (broken curve). Since the diffusivity of V_{Ba} in $BaTiO_3$ lattice, as investigated by Wernicke [29], is $D_{Ba} = 6.8 \times 10^{-2} \exp(-2.76\,\text{eV}/kT)$, the diffusion length of V_{Ba} is thus estimated to be 0.22 to 1.11 μm at 1000° C and is negligible at 600° C. Had the Daniels' model been true, there would be a depletion layer formed at the grain boundary regions such that the resistivity should be restored completely by 1000° C annealing, whereas it should not be changed by 600° C annealing, for the quenched samples. This is not the case. The outward diffusion of V_O is thus proposed to explain the formation of excess V_{Ba} during cooling.

The equilibrium concentrations of V_{Ba} and V_O, according to the law of mass action, are approximately the same and they are smaller when the samples are exposed to lower temperature. Diffusion of V_{Ba} and V_O toward the grain boundary are thus expected to occur. The diffusivity of barium vacancies (V_{Ba}) is, however, much lower than that of oxygen vacancies (V_O) so that the V_{Ba} can be approximately assumed frozen during the cooling process. Excess V_{Ba} thus

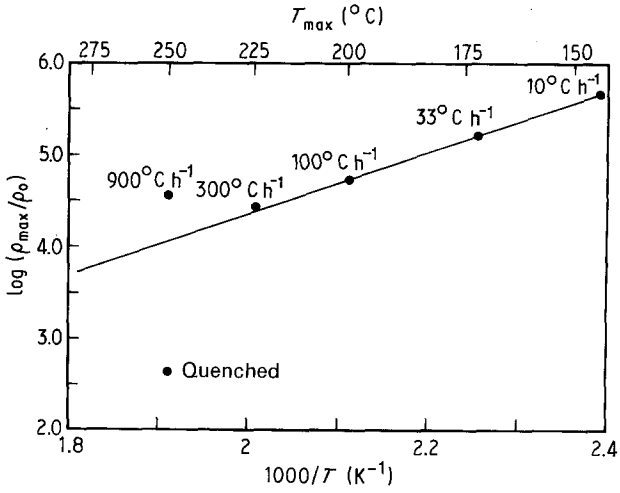

Figure 5 The plot of log (ρ_{max}/ρ_0) against $1/T_{max}$ of the 1350° C, 2 h sintered samples cooled at different rates.

results at the grain boundary region due to outward diffusion of V_O. Since the V_{Ba} can act as electron traps, a layer depleted in the charge carrier will result, which is as effective as the surface state of concentration N_s at forming a potential barrier ϕ. The slower the cooling rate, the larger the amount of excess V_{Ba} left over and hence the higher the potential barrier ϕ will be.

When the samples are annealed at 600° C for 40 min, after being cooled at room temperature, the equilibrium vacancy concentration is raised to a higher level. The oxygen vacancies (V_O) thereafter will diffuse inwardly and recombine with a proportion of excess barium vacancies (V_{Ba}). The equivalent surface state concentration N_s is lowered slightly and results in a smaller ρ_{max} value. As for the effect of annealing on the quenched samples, the existing concentrations of V_{Ba} and V_O correspond to the equilibrium values of the sintering temperature (1350° C) when the samples are quenched from that temperature. The annealing at 1000° C will certainly lower the oxygen vacancy concentration via outward diffusion of V_O leaving the frozen V_{Ba} behind. The ρ_{max} of the samples is thus expected to increase. Re-annealing at 600° C after the samples have been quenched from 1000° C will result in the same behaviour as shown in Fig. 4.

Even though the oxygen vacancy diffusion mechanism seems to be able to account for the observed cooling and annealing effect on the electrical resistivities of PTCR specimens qualitatively well, there still exists a discrepancy. The diffusion rate of oxygen vacancies (V_O) in $BaTiO_3$, according to the investigation by Wernicke [29], $D_O = 5.7 \times 10^3 \exp(-2.05\,\text{eV}/kT)$, which is enormous at high temperature. With such a high diffusivity, almost all of the V_O can diffuse to grain boundaries instantaneously during cooling, immaterial to the α_c value. The result will be grains excess in V_{Ba} everywhere which will render the materials insulating. The only remedy to such a discrepancy between the model and observed results is to assume that the diffusion of V_O is significantly slowed down due to some unknown mechanism. Formation of a defect complex which consists of a pair of barium and oxygen vacancies ($V_O^{\cdot\cdot}$–V_{Ba}'') bonded together is, therefore, proposed.

As the sample is cooled from the sintering temperature, the equilibrium values of V_{Ba} and V_O are lowered. Both of the vacancies have a tendency to diffuse towards the grain boundaries. The diffusion of V_{Ba} is slow and that of V_O is initially rapid. The excess barium vacancy (V_{Ba}) which is thermodynamically unfavourable, tends to capture the oxygen vacancy (V_O) and form a defect complex ($V_O^{\cdot\cdot}$–V_{Ba}''). The diffusion of V_O is significantly suppressed immediately after the formation of the $V_O^{\cdot\cdot}$–V_{Ba}'' complex since the oxygen vacancy must overcome the binding energy of the defect complex before it can diffuse. The result is that only the V_O sited at regions very close to the grain boundary have the chance to diffuse out. Thus only an ultra-thin layer of excess V_{Ba} region is formed and the electrical resistivity can be increased slightly.

When the samples are quenched from sintering temperature, the existence of frozen V_{Ba} and V_O is quite abundant. Both the vacancies experience the high energy state. They associate with each other easily and form the defect complex ($V_O^{\cdot\cdot}$–V_{Ba}''). As the temperature is raised again to the annealing temperature (1000° C), the outward diffusion of oxygen vacancies (V_O) is, thus, very slow. Consequently, the annealing process can only moderately modify the ρ_{max} value. It is worth noting that while the reoxidation of the materials owing to outward diffusion of V_O is retarded, the reduction of materials due to inward diffusion of oxygen vacancies is not expected to be affected markedly by the existence of a defect complex. This is in accord with the results observed by Jonker [18].

5. Conclusions

The electrical properties of PTC-type $BaTiO_3$ ceramics were varied by controlling the cooling or annealing processes. Owing to the similarity of the microstructures of each sample, the variation of PTCR behaviour can be ascribed solely as the influences of the defect chemistry of the materials.

1. The decrease of maximum and minimum resistivities (ρ_{max} and ρ_{min}) as the cooling rate increases from 10 to 300° C h^{-1} can be simply explained by Heywang's and Jonker's model.

2. The potential barrier is presumed to result from the existence of excess barium vacancies (V_{Ba}) near grain boundary regions, which are possibly due to the outward diffusions of the oxygen vacancies (V_O) to the grain boundaries during cooling.

3. The maximum potential barrier height (ϕ_{max}) of the samples is the same and can be deduced from the relationship between the ρ_{max} and corresponding temperature (T_{max}). It is estimated to be $\phi_{max} = 0.66$ eV.

4. The formation of a $V_O^{\cdot\cdot}$–V_{Ba}'' defect complex is proposed to explain the retardation of oxygen vacancy diffusion, which, in turn accounts for the phenomenon that the annealing can only affect the electrical properties moderately.

Acknowledgement

This work has been supported by the National Science Council under contracts NSC77-0404-E0003-01.

References

1. P. W. HAAYMAN, R. W. DAM and H. A. KLASENS, German Patent 929350, June (1955).
2. W. HEYWANG, *Solid State Electron.* **3** (1961) 51.
3. W. HEYWANG, *J. Amer. Ceram. Soc.* **47** (1964) 484.
4. G. H. JONKER, *ibid.* **7** (1964) 895.
5. W. T. PERIA, W. R. BRASTCHUM and R. D. FENITY, *ibid.* **44** (1961) 249.
6. J. B. MacCHESNEY and J. F. POTTER, *ibid.* **48** (1965) 81.
7. H. IHRIG and W. PUSHCHERT, *J. Appl. Phys.* **48** (1977) 3081.
8. J. DANIELS, K. H. HÄERDTL and R.WERNICKE, *Philips Technol. Rev.* **38** (1978/79) 73.
9. H. NEMOTO and I. ODA, *J. Amer. Ceram. Soc.* **63** (1980) 398.
10. G. B. LEWIS and C. R. A. CATLOW, *ibid.* **68** (1985) 555.
11. H. A. SAUER and J. R. FISHER, *ibid.* **44** (1961) 54.
12. P. K. GALLAGHER, F. SCHREY and F. V. DiMARCELLO, *ibid.* **46** (1963) 358.
13. H. UEOKA and M. YODOGAWA, *IEEE Trans. Mfg. Tech.* **MFT-3** (1974) 72.
14. M. KUWABARA, S. SUEMURA and M. KAWAHARA, *Amer. Ceram. Soc. Bull.* **64** (1985) 1394.
15. O. SABURI and K. WAKINO, *IEEE Trans. Comp. Parts* **CP-10** (1963) 53.
16. E. ANDRICH, *Elctron. Appl.* **26** (1965/66) 123.
17. T. MATSUOKA *et al.*, *J. Amer. Ceram. Soc.* **55** (1972) 108.
18. G. H. JONKER, in "Advances in Ceramics", Vol. 1, edited by L. M. Levinson (The American Ceramic Society, Columbus, Ohio, 1981) p. 155.
19. W. HEYWANG, *J. Mater. Sci.* **6** (1971) 1214.
20. T. FUKAMI and H. TSUCHIYA, *Jpn J. Appl. Phys.* **18** (1979) 735.
21. H. IHRIG, *J. Amer Ceram. Soc.* **64** (1981) 617.
22. M. KUWABARA, *ibid.* **64** (1981) C-170.
23. T. ASHIDA and H. TOYODA, *Jpn J. Appl. Phys.* **5** (1966) 269.
24. R. N. BASU and H. S. MAITI, *Mater. Lett.* **5** (1987) 99.
25. I. UEDA and S. IKEGAMI, *J. Phys. Soc. Jpn* **20** (1965) 546.
26. M. KHAN, *Amer. Ceram. Soc. Bull.* **50** (1971) 677.
27. Y. MATSUO *et al.*, *ibid.* **47** (1968) 292.
28. R. N. BASU and H. S. MAITI, in Proceedings of the IEEE 6th ISAF., Bethlehem, PA, USA, June 1986, (IEEE, New York, 1986) p. 685.
29. R. WERNICKE, *Philips Res. Rep.* **31** (1976) 526.

Received 7 April
and accepted 16 August 1989